# Chapter 3

# Efficient Refinement: Edge-Smoothing Weighted Guided Image Filter

## 3.1 Background

Generally, the transmission map refinement process can be achieved by using an edge-preserving filters. These filters refine the transmission map efficiently and resulting in smoother, higher-quality edge details. They reduce noise from an image while preserving and enhancing the edges. They provide more accurate calibration of the transmission map and a more detailed description of the transmission profile. The existing guided image filter (GIF) [49], weighted guided image filter (WGIF) [50], gradient domain guided image filter (GGIF) [51], and effective guided image filter (EGIF) [52] are popular and good edge-preserving filters. However, the main

limitations of the existing edge-preserving filters are the fixed regularization parameter, single scale edge-weighting constraint and local linear transform model. They remove gradient reversal artifacts and halos artifacts. However, over-smoothing and color distortion persist in the sharp regions.

In this Chapter, we proposed an effective scale-aware edge-smoothing weighting constraint-based weighted guided image filter. Further, the proposed filter is used in single image dehazing application. The qualitative and quantitative analysis of the proposed method with the existing dehaze methods are tested on different datasets and their comparative analysis are presents in detail in this Chapter.

### 3.1.1 Major contributions of the work

The novelties and major contributions of this chapter are as follows:

- We proposed a new effective scale-aware edge-smoothing weighting constraint-based weighted guided image filter (ESAESWC-WGIF) to refine the transmission map efficiently. The objective of this filter is to refine the transmission map accurately and preserves edge information effectively.
- This edge-preserving filter is proposed by incorporating an effective scale-aware edge-smoothing weighting constraint (ESAESWC) in the cost function of guided image filter (GIF) [49].
- The proposed filter is a multi-scale and local linear model-based edge-preserving filter. This filter is less sensitive to the regularization parameter than the existing GIF [49], WGIF [50], GGIF [51], and EGIF [52] algorithms.
- ESAESWC-WGIF is an excellent edge-preserving smoothing filter. It removes halos, over-smoothing effects strongly and preserves edge information more

accurately than the existing GIF [49], WGIF [50], GGIF [51], and EGIF [52] algorithms.

## 3.2 Effective Scale-Aware Edge-Smoothing Weighting Constraint-Based Weighted Guided Image Filter

In this section, a new effective scale-aware edge-smoothing weighting constraint is first proposed. Next, it is incorporated into the cost function of guided image filter (GIF) [49] to form effective edge-preserving filter.

### 3.2.1 A New Edge-Smoothing Weighting Constraint

The proposed edge-smoothing weighting $\overline{\psi}_I(k)$ is multi-scale and it is defined by using local variance of both $3 \times 3$ and $(2\zeta_1 + 1) \times (2\zeta_1 + 1)$ pixel windows in the guidance image $I$ as follows:

$$\overline{\psi}_I(k) = \frac{\sigma_{I,1}(k)}{\overline{\sigma}^2}, \tag{3.1}$$

and $\overline{\sigma}^2$ is expressed as:

$$\overline{\sigma}^2 = \frac{1}{N} \sum_{k=1}^{N} {\sigma^2}_{I,\,\zeta_1}(k). \tag{3.2}$$

where $N$ indicates total pixel count in the guidance image $I$, $\sigma_{I,1}(k)$ and ${\sigma^2}_{I,\,\zeta_1}(k)$ are the local variance of $I$ in $3 \times 3$ window and $(2\zeta_1 + 1) \times (2\zeta_1 + 1)$ window of all pixels.

### 3.2.2 The Proposed Filter

In this section, a newly proposed edge-aware weighting constraint $\overline{\psi}_I(k)$ is incorporated into the cost function of GIF [49]. The cost function in the proposed filter is minimized by linear ridge regression model [63, 64]. The values of linear coefficients $a_k$ and $b_k$ are evaluated by minimizing the cost function $E(a_k, b_k)$ in the window $\omega_{\zeta_1}(k)$ as:

$$E(a_k, b_k) = \sum_{i(x,y)\in\omega_{\zeta_1}(k)} \{(a_k I_{\mathrm{i}} + b_k - p_i)^2 + a_k^2 \frac{\varepsilon}{\overline{\psi}_I(k)}\}. \tag{3.3}$$

The cost function in (3.3) represents a linear ridge regression model [63, 64]. Its solution is obtained in terms of two optimized linear constants: $a_k$ and $b_k$. They can be expressed as:

$$a_k = \frac{\mu_{I*p,\zeta_1}(k) - \mu_{I,\,\zeta_1}(k)\mu_{p,\,\zeta_1}(k)}{{\sigma^2}_{I,\,\zeta_1}(k) + \frac{\varepsilon}{\overline{\psi}_I(k)}}, \tag{3.4}$$

and

$$b_k = \mu_{p,\,\zeta_1}(k) - a_k \mu_{I,\,\zeta_1}(k). \tag{3.5}$$

Here, $\varepsilon$ is a regularization parameter which penalizing large $a_k$ value. In this work, we assumed $I$ and $p$ are identical as in GIF [49] for simple and better analysis. After simplification can be expressed as:

$$\mu_{I*p,\zeta_1}(k) - \mu_{I,\,\zeta_1}(k)\mu_{p,\,\zeta_1}(k) = {\sigma^2}_{I,\,\zeta_1}(k) \tag{3.6}$$

and

$$\mu_{p,\,\zeta_1}(k) = \mu_{I,\,\zeta_1}(k). \tag{3.7}$$

After substituting (3.6) and (3.7) in (3.4), we obtain:

$$a_k = \frac{{\sigma^2}_{I,\,\zeta_1}(k)}{{\sigma^2}_{I,\,\zeta_1}(k) + \frac{\varepsilon}{\overline{\psi}_I(k)}}, \tag{3.8}$$

and

$$b_k = (1 - a_k)\mu_{I,\,\zeta_1}(k), \tag{3.9}$$

After dividing (3.8) by $\sigma^2{}_{I,\,\zeta_1}(k)$, we get:

$$a_k = \frac{1}{1 + \varepsilon \frac{1}{\sigma^2{}_{I,\,\zeta_1}(k)\overline{\psi}_I(k)}}. \tag{3.10}$$

Substituting value of $\overline{\psi}_I(k)$ from (3.1) into (3.10)

$$a_k = \frac{1}{1 + \varepsilon \frac{1}{\left\{\sigma^2{}_{I,\,\zeta_1}(k)\right\}.\left\{\frac{\sigma_{I,1}{}^{(k)}}{\overline{\sigma}^2}\right\}}} \tag{3.11}$$

$$a_k = \frac{1}{1 + \varepsilon \frac{\overline{\sigma}^2}{\sigma^2{}_{I,\,\zeta_1}(k).\sigma_{I,1}(k)}}. \tag{3.12}$$

Finally, $q_i$ is expressed as:

$$q_i = \frac{1}{|\omega_{\zeta_1}(k)|} \sum_{k \in \omega_{\zeta_1}(k)} (a_k I_i + b_k), \tag{3.13}$$

$$q_i = (\overline{a}_i I_i + \overline{b}_i), \tag{3.14}$$

where $\overline{a}_i$ and $\overline{b}_i$ terms in the above expression represent mean of $a_k$ and $b_k$, respectively in the corresponding window of all pixels and it is computed as:

$$\overline{a}_i = \frac{1}{|\omega_{\zeta_1}(k)|} \sum_{k \in \omega_{\zeta_1}(k)} a_k, \tag{3.15}$$

$$\overline{b}_i = \frac{1}{|\omega_{\zeta_1}(k)|} \sum_{k \in \omega_{\zeta_1}(k)} b_k. \tag{3.16}$$

In order to preserve edge information in sharp regions, $a_k$ should be 1 and $b_k$ close to 0; whereas for smooth regions $a_k$ should be close to 0 and $b_k$ should be 1 [50].

## 3.3 Application of The Proposed Filter in Single Image Dehazing

Image dehazing is a process that removes haze from an image. It is used to improve the visual quality of hazy image by removing the blurriness caused by the presence of haze. The edge-preserving filter use transmission map refinement process to remove haze. Here, we present application of the proposed filter in haze removal. The basic flow diagram of the proposed ESAESWC-WGIF is shown in Figure 3.1. This algorithm has following three steps:

- First, calculate the atmospheric map and initial transmission map by using dark channel prior (DCP) [15].
- Next, refine the initial transmission map by using the proposed ESAESWC-WGIF algorithm. This filter removes halo artifacts and over-smoothing effect strongly and preserve edge information more accurately than the existing filters.
- Finally, restore the dehazed image from the scene radiance.

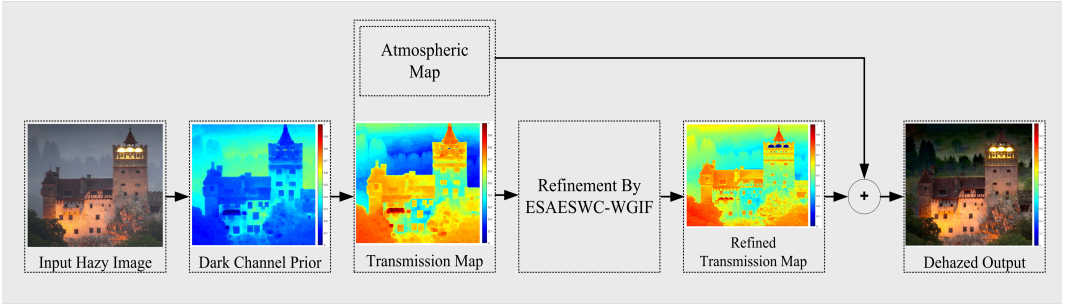


FIGURE 3.1: The basic framework of the proposed haze removal method.

### 3.3.1 Dark Channel Prior (DCP)

We estimate the atmospheric map and initial transmission map using dark channel prior (DCP) [15] method. McCartney [91] represents formation of haze mathematically as:

$$I(x) = J(x)t(x) + A(1 - t(x)), \tag{3.17}$$

where $x$ is pixel's position into the image, $I(x)$ is input hazy image, $J(x)$ is output dehazed image or scene radiance, $t(x)$ is the medium transmission map, and $A$ is the global atmospheric light or map. In (3.17), the first term $J(x)t(x)$ and the second term $A(1 - t(x))$ are called direct attenuation and air-light, respectively.

The relation of medium transmission map $t(x)$ with the object's distance $d(x)$ can be expressed as:

$$t(x) = exp(1 - \beta d(x)) \leq 1, \tag{3.18}$$

where $0 \leq d(x) \leq \infty$ is the depth (distance) of scene-point (pixel) from camera and $\beta$ is the scattering coefficient related to the wavelength of light and it is exponentially attenuated with the scene depth $d(x)$. The single image haze removal result can be obtained by putting $t(x)$ and $A$ value in (3.17).

According to dark channel prior (DCP) [15] method, $J$ can be estimated after assuming some prior information. In DCP, dark pixel (lowest pixel) concept is used to calculate transmission map $t(x)$ and $A(x)$ and the atmospheric map $A$ is estimated by selecting top 0.1% of brightest pixels in hazy image. For a given atmospheric map $A$, (3.17) can be modified as:

$$\frac{I^c(x)}{A^c} = t(x)\frac{J^c(x)}{A^c} + 1 - t(x), \tag{3.19}$$

where $c$ denotes color channels $(r, g, b)$. $A^c$ and $J^c$ represent the atmospheric map and dehaze image for color channel, respectively. Due to constant behaviour of

transmission map $t(x)$ in a local patch $\Omega(x)$, it is denoted by $\tilde{t}(x)$ [15]. Dark channel is computed after substituting the minimum operator on both sides of (3.19).

$$\min_{y\in\Omega(x)}\Big(\min_{c\in\{r,g,b\}}\frac{I^c(y)}{A^c}\Big)=\tilde{t}(x)\min_{y\in\Omega(x)}\Big(\min_{c\in\{r,g,b\}}\frac{J^c(y)}{A^c}\Big)+1-\tilde{t}(x). \tag{3.20}$$

According to DCP [15], to restore the scene radiance $J$ as haze-free image, the dark channel of the scene radiance should be zero and it can be expressed as:

$$J^{dark}(x)=\min_{y\in\Omega(x)}\Big(\min_{c}\frac{J^c(y)}{A^c}\Big)=0, \tag{3.21}$$

where $J^{dark}$ is the scene radiance for dark channel. Since $A^c$ should be always positive and (3.20) can be modified as:

$$\min_{y\in\Omega(x)}\Big(\min_{c}\frac{I^c(y)}{A^c}\Big)=1-\tilde{t}(x). \tag{3.22}$$

After simplification, $\tilde{t}(x)$ can be expressed as:

$$\tilde{t}(x)=1-\min_{y\in\Omega(x)}\Big(\min_{c}\frac{I^c(y)}{A^c}\Big). \tag{3.23}$$

As we know that the DCP method is not valid for large sky, sea or white regions because the color of sky or ocean during haze are mostly similar to atmospheric map. Due to that the transmission map becomes close to 0 [15, 26, 62]. Finally, the transmission map can be expressed as:

$$\tilde{t}(x)=1-w\min_{y\in\Omega(x)}\Big(\min_{c}\frac{I^c(y)}{A^c}\Big). \tag{3.24}$$

Here, a constant parameter $w$ $(0<w\leq 1)$ is used to retain a very limited amount of haze for distant objects.

### 3.3.2 Transmission Map Refinement

Next, the following expression can be used to refine the initial transmission map $\tilde{t}(x)$ as:

$$q_i = \overline{t}(x) = (\overline{a}_i I_i + \overline{b}_i), \tag{3.25}$$

where $\overline{t}(x)$ represent refined transmission map (filtered output).

### 3.3.3 Restore Dehaze Image

Finally, the dehazed output image can be calculated by the following expression as:

$$J^c(x) = \frac{I^c(x) - A^c}{max(\overline{t}(x), t_0)} + A^c. \quad c \in (r, g, b) \tag{3.26}$$

where the value of $t_0$ is set to 0.1 as in [49] to avoid noise amplification.

## 3.4 Experimental Results and Analysis

The performance of the proposed method and the existing methods are experimented and evaluated using Matlab R2018a on a PC with Intel (R) Core (TM) i7-6700 CPU @ 3.40 GHz of a 64-bit operating system with RAM-8GB. The proposed algorithm is tested on about 3200 hazy, non-hazy and synthetic images from Fattal [16], NYU2 [66], D-HAZY [65], Haze-RD [69], O-HAZE [71] datasets and the outcomes are compared with 7 state-of-the-art haze removal methods out of which DCP [15] is prior based dehazing methods, GIF [49], WGIF [50], GGIF [51], EGIF [52] are four edge-preserving image dehazing filters and DehazeNet [37], RYF-Net [39] are two deep-learning based image dehazing methods. This section presents the

qualitative and quantitative analysis of the proposed algorithm with the existing dehaze methods.

### 3.4.1 Dataset

The performance of the proposed algorithm is tested on about 3200 images from indoor real hazy, outdoor real hazy, synthetic hazy of different datasets viz. Fattal [16], NYU2 [66], D-HAZY [65], Haze-RD [69], O-HAZE [71].

### 3.4.2 Qualitative Analysis

The outcomes of the proposed algorithm for different datasets are compared with 7 state-of-the-art DCP [15], GIF [49], WGIF [50], GGIF [51], EGIF [52] DehazeNet [37], and RYF-Net [39] methods for effective visual analysis. The refined transmission map of the proposed algorithm and different existing GIF [49], WGIF [50], GGIF [51], EGIF [52] methods are evaluated and their comparative results are shown in Figure 3.2. As we can see clearly from Figure 3.2 that the dehazed outcomes corresponding to the refined $\bar{t}(x)$ of the proposed method remove haze more efficiently than the existing edge -preserving filters. Next, the dehazed result of the proposed method and the existing DCP [15], GIF [49], WGIF [50], GGIF [51], EGIF [52], DehazeNet [37] and RYF-Net [39] methods are evaluated for five benchmark hazy images of different datasets and their comparative outcomes are shown in Figure 3.3 to Figure 3.7, respectively. It is clear from Figure 3.3 to Figure 3.7 that the proposed method removes halos, over-smoothing strongly and preserves edge information more precisely in both flat and sharp regions than the existing DCP [15], GIF [49], WGIF [50], GGIF [51], EGIF [52], DehazeNet [37] and RYF-Net [39] methods.

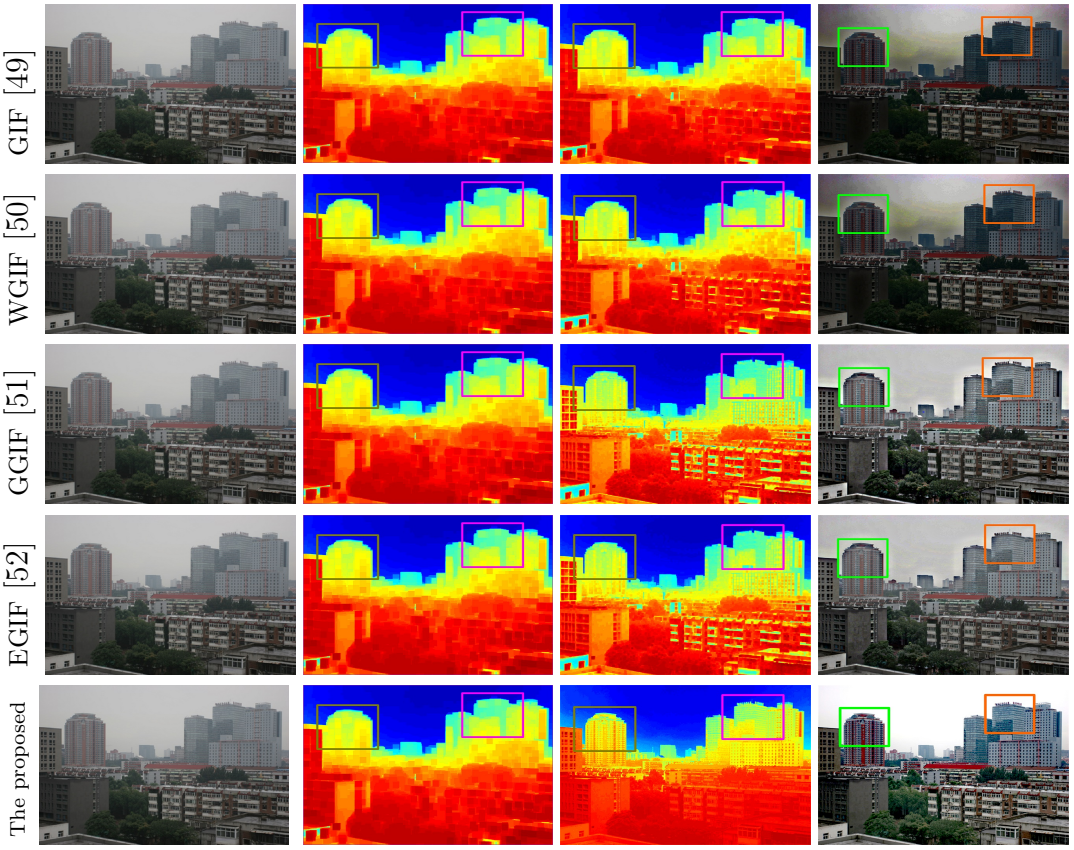


FIGURE 3.2: Refined transmission maps of different edge-preserving filters.

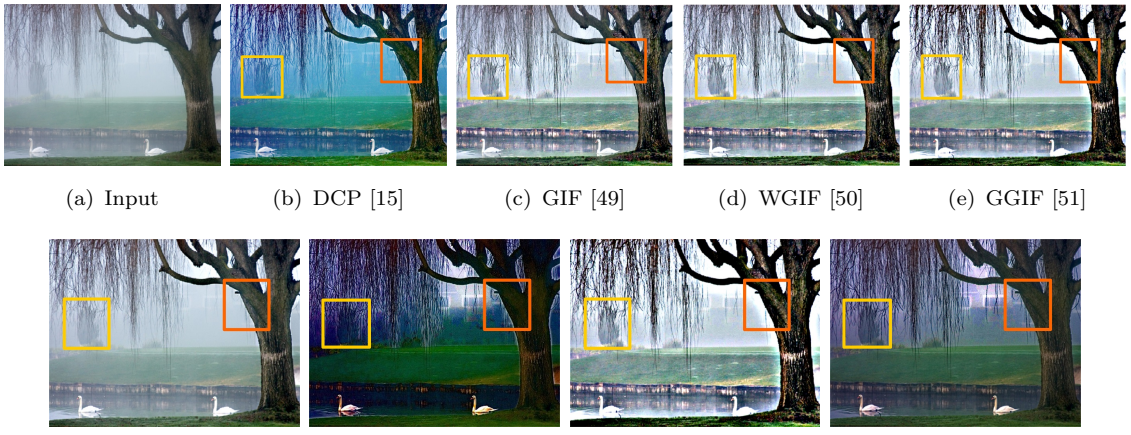


FIGURE 3.3: Dehazed outcomes of different haze removal methods.

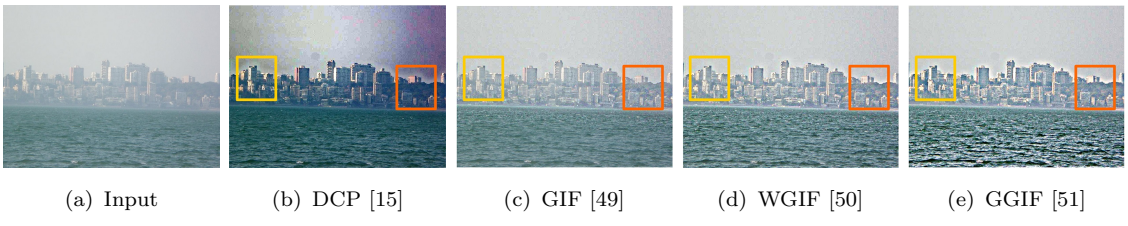

(a) Input (b) DCP [15] (c) GIF [49] (d) WGIF [50] (e) GGIF [51]

(f) EGIF [52] (g) DehazeNet [37] (h) RYF-Net [39] (i) The proposed

FIGURE 3.4: Dehazed outcomes of different haze removal methods.

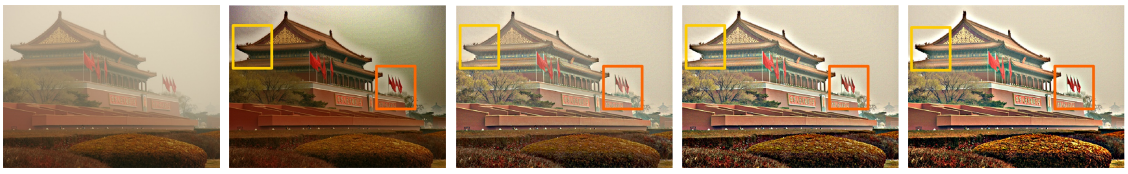

(a) Input (b) DCP [15] (c) GIF [49] (d) WGIF [50] (e) GGIF [51]

(f) EGIF [52] (g) DehazeNet [37] (h) RYF-Net [39] (i) The proposed

FIGURE 3.5: Dehazed outcomes of different haze removal methods.

### 3.4.3 Quantitative Analysis

The objective evaluation of the proposed filter is compared with the existing GIF [49], WGIF [50], GGIF [51] and EGIF [52] methods using an effective blind object image quality metric [83]. Score of these filters are calculated for different values of the regularization parameter $\varepsilon$ and their values are listed in Table 3.1. As we can seen clearly from Table 3.1 that the scores of GIF [49] and WGIF [50] initially increase and then decrease for large $\varepsilon$ value. However, GGIF [51] and EGIF [52]

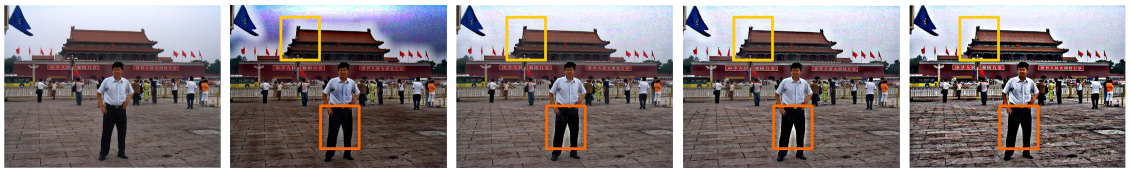

(a) Input (b) DCP [15] (c) GIF [49] (d) WGIF [50] (e) GGIF [51]

(f) EGIF [52] (g) DehazeNet [37] (h) RYF-Net [39] (i) The proposed

FIGURE 3.6: Dehazed outcomes of different haze removal methods.

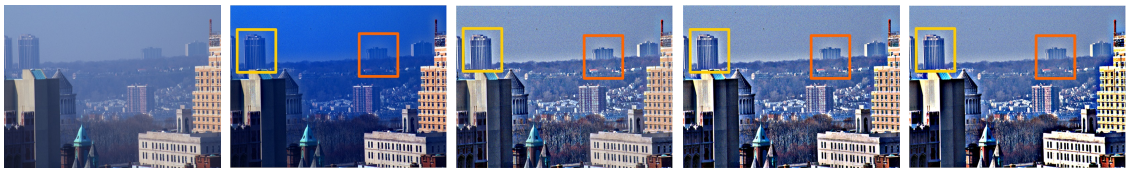

(a) Input (b) DCP [15] (c) GIF [49] (d) WGIF [50] (e) GGIF [51]

(f) EGIF [52] (g) DehazeNet [37] (h) RYF-Net [39] (i) The proposed

FIGURE 3.7: Dehazed outcomes of different haze removal methods.

both have higher scores than GIF [49] and WGIF [50] but they also generate lower scores for large $\varepsilon$ values ($\varepsilon = 0.4^2, 0.8^2$), whereas the scores of the proposed method increase with the increase of $\varepsilon$ and it decreases slightly even for large $\varepsilon$ values.

The performance metrics: PSNR [87], SSIM [86], FADE [81] and CIEDE2000 [89] of the proposed method and the existing dehaze methods are evaluated for natural hazy, non-hazy and synthetic images from Fattal [16], NYU2 [66], D-HAZY [65], Haze-RD [69], O-HAZE [71] datasets. For the best performance, PSNR [87] and

SSIM [86] values must be higher, whereas FADE [81] and CIEDE2000 [89] values must be lower. These results are furnished in Table 3.2 to Table 3.6.

The blue bold face values in each row indicate best measured value. PSNR [87] and SSIM [86] values of EGIF [52], DehazeNet [37] and RYF-Net [39] methods are comparable and usually, these values are low for DCP [15] GIF [49], WGIF [50], GGIF [51] methods. Next, RYF-Net [39] is more comparable method which is capable of retaining structures more accurately than the rest of existing methods. FADE [81] and CIEDE2000 [89] values should be small for a better image dehazing. However, these values are higher in DCP [15] GIF [49], WGIF [50], GGIF [51], and EGIF [52] methods. Usually, deep learning-based DehazeNet [37], and RYF-Net [39] methods produced more comparable FADE [81] values than the existing DCP [15] GIF [49], WGIF [50], GGIF [51], EGIF [52] methods and similar is the case for CIEDE2000 [89] metric scores.

It is clear from Table 3.2 to Table 3.6 that for all the aforesaid datasets the PSNR and SSIM values of the proposed method are higher than rest of the existing methods, as expected. The FADE values are the least for all the datasets with the proposed method, as expected and CIEDE2000 metric values are also the least for Fattal [16], NYU2 [66], Haze-RD [69], and O-HAZE [71] datasets except D-HAZY [65] dataset. This entails that the proposed method is better than the existing dehaze methods. Next, the average execution time of the proposed method and the existing DCP, GIF, WGIF, GGIF, EGIF, DehazeNet, and RYF-Net methods are computed for five benchmark hazy images having resolution $250 \times 200$, $550 \times 400$, $850 \times 600$, $1000 \times 950$ and $1400 \times 1200$ and listed in Table 3.7. These results prove that the proposed method and deep learning based DehazeNet [37], RYF-Net [39] methods execute faster than the rest of the methods. It is clear from this table that the proposed method not only dehaze images of various resolution faster but it is faster

than the fastest existing methods also. The statistical analysis of quality metrics PSNR [87], SSIM [86], FADE [81] and CIEDE2000 [89] for the proposed method and the existing DCP [15] GIF [49], WGIF [50], GGIF [51], EGIF [52], DehazeNet [37], RYF-Net [39] methods are represented by box plot [92] shown in Figure 3.8(a)-(d), respectively. It is clear from the box plot figures that the proposed method has higher median value for PSNR [87] and SSIM [86], whereas lower median value for FADE [81] and CIEDE2000 [89] metrics in comparison to other existing methods. The horizontal line within the box plot represents median value. Thus, it proves that the proposed method provide better dehaze outcomes than the existing DCP [15] GIF [49], WGIF [50], GGIF [51], EGIF [52], DehazeNet [37], RYF-Net [39]. Finally, it is proved from Figure 3.2 to Figure 3.8 and Table 3.1 to Table 3.7 that the proposed method removes halo artifacts, over smoothing strongly and preserves edge information more accurately than the existing DCP [15] GIF [49], WGIF [50], GGIF [51], EGIF [52], DehazeNet [37] and RYF-Net [39] methods in both regions. Moreover, the proposed method is fast and preserves edge informations in sharp region more accurately as compared to the existing haze removal methods.

TABLE 3.1: Objective evaluation on image shown in Fig. 3.3

| | GIF [49] | WGIF [50] | GGIF [51] | EGIF [52] | The proposed |
|---|---|---|---|---|---|
| Input | 36.87 | 36.87 | 36.87 | 36.87 | 36.87 |
| $\varepsilon = 0.001^2$ | **39.64** | 38.19 | 39.22 | 39.07 | 39.45 |
| $\varepsilon = 0.05^2$ | 41.36 | 42.19 | 45.38 | 46.52 | **46.85** |
| $\varepsilon = 0.1^2$ | 35.67 | 37.46 | 45.15 | 46.23 | **46.72** |
| $\varepsilon = 0.4^2$ | 31.26 | 32.91 | 43.69 | 44.51 | **46.57** |
| $\varepsilon = 0.8^2$ | 27.35 | 29.87 | 42.53 | 43.66 | **46.19** |

TABLE 3.2: Performance comparison on Fattal dataset

| Methods | PSNR | SSIM | FADE | CIEDE2000 |
|---|---|---|---|---|
| DCP [15] | 17.38 | 0.7514 | 2.725 | 25.57 |
| GIF [49] | 19.51 | 0.7826 | 2.101 | 21.16 |
| WGIF [50] | 20.08 | 0.8205 | 1.686 | 18.26 |
| GGIF [51] | 23.44 | 0.8519 | 1.295 | 15.08 |
| EGIF [52] | 27.69 | 0.8835 | 0.817 | 11.55 |
| DehazeNet [37] | 27.91 | 0.8806 | 0.779 | 9.68 |
| RYF-Net [39] | 29.58 | 0.9013 | 0.795 | 7.93 |
| The proposed | **31.07** | **0.9291** | **0.508** | **5.18** |

TABLE 3.3: Performance comparison on NYU2 dataset

| Methods | PSNR | SSIM | FADE | CIEDE2000 |
|---|---|---|---|---|
| DCP [15] | 19.05 | 0.7794 | 2.475 | 23.48 |
| GIF [49] | 21.64 | 0.7906 | 2.086 | 20.05 |
| WGIF [50] | 22.59 | 0.8139 | 1.839 | 19.17 |
| GGIF [51] | 24.77 | 0.8662 | 1.416 | 16.38 |
| EGIF [52] | 27.14 | 0.8791 | 1.142 | 12.66 |
| DehazeNet [37] | 28.06 | 0.8838 | 1.119 | 10.01 |
| RYF-Net [39] | 29.27 | 0.9171 | 1.053 | 8.25 |
| The proposed | **31.69** | **0.9307** | **0.865** | **6.64** |

TABLE 3.4: Performance comparison on D-HAZY dataset

| Methods | PSNR | SSIM | FADE | CIEDE2000 |
|---|---|---|---|---|
| DCP [15] | 22.69 | 0.8105 | 2.681 | 29.07 |
| GIF [49] | 23.95 | 0.8183 | 2.135 | 25.49 |
| WGIF [50] | 24.72 | 0.8371 | 1.861 | 21.64 |
| GGIF [51] | 25.08 | 0.8509 | 1.497 | 18.25 |
| EGIF [52] | 27.43 | 0.8769 | 1.005 | 15.31 |
| DehazeNet [37] | 28.79 | 0.8841 | 1.169 | 11.97 |
| RYF-Net [39] | **29.88** | **0.9215** | 0.985 | **7.03** |
| The proposed | 28.15 | 0.8803 | **0.837** | 8.11 |

TABLE 3.5: Performance comparison on Haze-RD dataset

| Methods | PSNR | SSIM | FADE | CIEDE2000 |
|---|---|---|---|---|
| DCP [15] | 20.41 | 0.7837 | 2.208 | 27.51 |
| GIF [49] | 21.86 | 0.8065 | 1.964 | 23.86 |
| WGIF [50] | 24.72 | 0.8214 | 1.558 | 20.94 |
| GGIF [51] | 25.08 | 0.8468 | 1.163 | 17.25 |
| EGIF [52] | 29.88 | 0.8739 | 0.927 | 14.08 |
| DehazeNet [37] | 31.38 | 0.8815 | 0.862 | 11.73 |
| RYF-Net [39] | 32.04 | 0.9128 | 0.895 | 7.39 |
| The proposed | **34.05** | **0.9411** | **0.649** | **4.15** |

TABLE 3.6: Performance comparison on O-HAZE

| Methods | PSNR | SSIM | FADE | CIEDE2000 |
|---|---|---|---|---|
| DCP [15] | 21.15 | 0.8059 | 2.351 | 24.51 |
| GIF [49] | 23.09 | 0.8471 | 2.068 | 21.93 |
| WGIF [50] | 23.87 | 0.8609 | 1.885 | 17.02 |
| GGIF [51] | 25.96 | 0.8673 | 1.375 | 13.16 |
| EGIF [52] | 28.74 | 0.9045 | 1.028 | 9.94 |
| DehazeNet [37] | 28.91 | 0.9004 | 0.993 | 7.68 |
| RYF-Net [39] | 30.05 | 0.9159 | 0.975 | 5.03 |
| The proposed | **30.61** | **0.9536** | **0.731** | **3.15** |

TABLE 3.7: Execution time (in sec.) based Assessment

| Methods | Fig.3.3 250×200 | Fig.3.4 550×400 | Fig.3.5 850×600 | Fig.3.6 1000×950 | Fig.3.7 1200×1400 | Average |
|---|---|---|---|---|---|---|
| DCP [15] | 18.27 | 21.95 | 26.64 | 30.55 | 39.92 | 27.46 |
| GIF [49] | 11.06 | 16.47 | 20.19 | 24.38 | 32.15 | 20.85 |
| WGIF [50] | 7.34 | 12.51 | 18.52 | 20.09 | 27.06 | 17.10 |
| GGIF [51] | 4.71 | 9.62 | 15.08 | 17.45 | 21.54 | 13.68 |
| EGIF [52] | 1.64 | 6.39 | 10.91 | 13.92 | 18.16 | 10.20 |
| DehazeNet [37] | 1.38 | 5.05 | 8.35 | 10.37 | 14.39 | 7.908 |
| RYF-Net [39] | 1.15 | 3.16 | 4.15 | 8.09 | 11.61 | 5.632 |
| The Proposed | **1.07** | **1.27** | **3.79** | **5.27** | **9.07** | **4.046** |

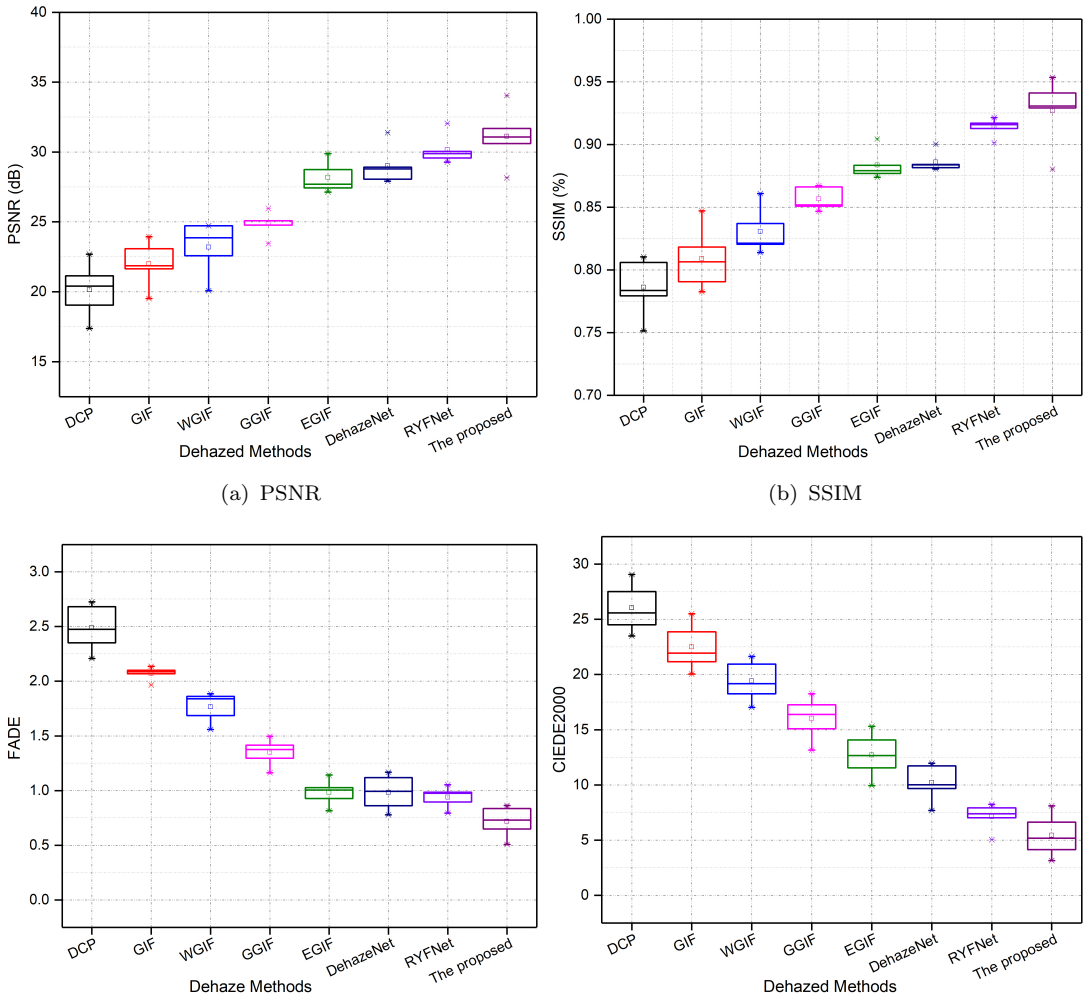


(a) PSNR (b) SSIM

(c) FADE (d) CIEDE2000

FIGURE 3.8: Dehazed outcomes of different haze removal methods.

## 3.5 Limitations

Due to limited visibility and poor contrast the proposed method fail in case of dense haze and night-time hazy conditions. The failure case of the proposed method and the existing DCP, GIF, WGIF, GGIF, EGIF, DehazeNet, RYF-Net methods on dense haze dataset [74] and night-time haze dataset [78] are shown in Figure 3.9 and Figure 3.10, respectively.

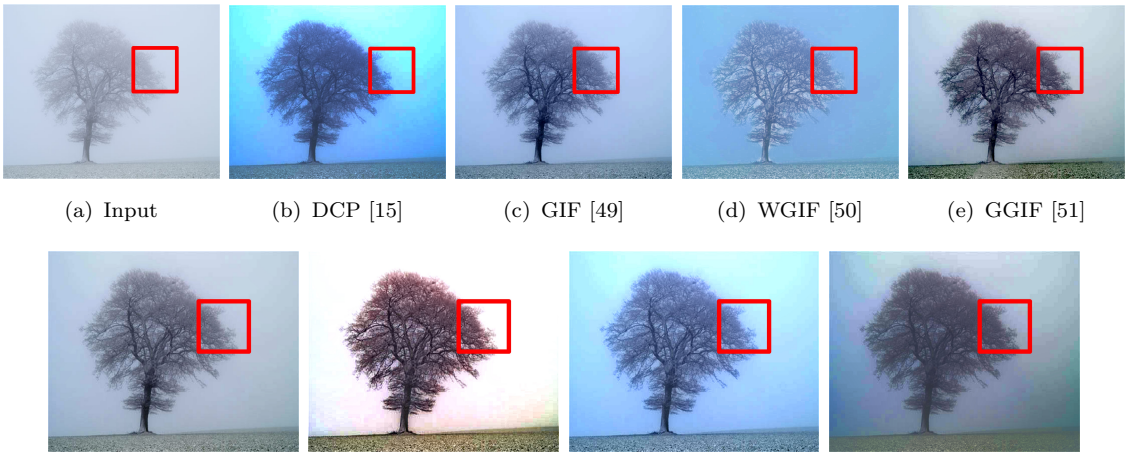

(a) Input (b) DCP [15] (c) GIF [49] (d) WGIF [50] (e) GGIF [51]

(f) EGIF [52] (g) DehazeNet [37] (h) RYF-Net [39] (i) The proposed

FIGURE 3.9: Dehazed outcomes on dense hazy images.

(a) Input (b) DCP [15] (c) GIF [49] (d) WGIF [50] (e) GGIF [51]

(f) EGIF [52] (g) DehazeNet [37] (h) RYF-Net [39] (i) The proposed

FIGURE 3.10: Dehazed outcomes on night-time hazy images.

## 3.6 Concluding Remarks

In this chapter, we present a new effective scale-aware edge-smoothing weighting constraint-based edge-smoothing weighted guided image filter (ESAESWC-WGIF) for single image dehazing. It is a multi-scale local linear transform model based edge-smoothing filter. This filter refines the transmission map more accurately than the existing image filters. It removes halos, over-smoothness strongly and preserves edge information precisely in sharp regions. The proposed algorithm is tested on about

3,200 images from real time hazy, non-real time hazy, synthetic hazy, dense hazy and night time hazy images of Fattal [16], NYU2 [66], D-HAZY [65], Haze-RD [69], O-HAZE [71] datasets and resulting outcomes are compared with 7 state-of-the-art DCP [15], GIF [49], WGIF [50], GGIF [51], EGIF [52], DehazeNet [37] and RYF-Net [39] methods. The comparative visual results shown in Figure 3.3 to Figure 3.7 prove that the proposed method has better color, contrast and visual quality than the rest of the methods. To analysis the enhancement feature of the restored image, a blind object evaluation metric is used to calculate score of the proposed filter and the existing GIF, WGIF, GGIF and EGIF methods for different values of the regularization parameter $\varepsilon$ and their values are listed in Table 3.1. It is clear from Table 3.1 that the scores of the proposed method increase with the increase of $\varepsilon$ and it decreases slightly even for large $\varepsilon$ values. We evaluated performance parameters such as PSNR [87], SSIM [86], FADE [81] and CIEDE2000 [89] metrics of the proposed method and the existing DCP [15] GIF [49], WGIF [50], GGIF [51], EGIF [52], DehazeNet [37], RYF-Net [39] methods on Fattal, NYU2, D-HAZY, Haze-RD, and O-HAZE datasets and their comparative results are are furnished in Table 3.2 to Table 3.6. The experimental results prove that the proposed method restore the images with excellent visual quality. Moreover, the proposed method is independent of the nature of the input image. It performs equally well for all datasets as compared to the existing dehaze methods. It is noteworthy that the proposed method is faster than the existing methods for a given resolution of images.